Effect of Solvent and pH on the Structure of PAMAM Dendrimers

Prabal K. Maiti,† Tahir Çağın,‡ Shiang-Tai Lin, and William A. Goddard, III*

Materials and Process Simulation Center, California Institute of Technology, Pasadena, California 91125

Received April 28, 2004; Revised Manuscript Received October 19, 2004

ABSTRACT: We report various structural and conformational properties of generations 4, 5, and 6 PAMAM (polyamidoamine) dendrimer [EDA (ethylenediamine) core)] at various protonation levels through extensive molecular dynamics (MD) simulations in explicit solvent. The presence of solvent leads to swelling of the dendrimer (by 33% for G5 compared to the case of no solvent). We find that decreasing the solution from high pH (∼10, no protonation) to neutral (∼7, only primary amines protonated) to low pH (∼4, tertiary amines also protonated) changes the radius of gyration of G5 from 21 to 22 to 25 Å, respectively. We also report such other structural quantities as radial density, distribution of terminal groups, solvent accessible surface area and volume, shape, and structure factors (to compare with SAXS and SANS experiments) at various pH conditions. *We find significant back-folding of the outer subgenerations in the interior of the molecules at all levels of pH, contrary to original expectations and some SANS experiments but in agreement with other SANS experiments.* We find significant water penetration inside the dendrimer, with ∼3 water/tertiary amine for high pH and ∼6 water/tertiary amine for low pH (all for G5). This indicates that the interior of the dendrimer is quite open with internal cavities available for accommodating guest molecules, suggesting using PAMAM dendrimer for guest−host applications. This estimate of internal waters suggests that sufficient water is available to facilitate metal ion binding.

1. Introduction

PAMAM dendrimers have primary amine groups at each branch end and tertiary amine groups at each branching point. As the dendrimer generation g is increased, Table 1 shows that the number of primary amines grows as $N = cm^g$ and the number of tertiary amines grows as $N = cm^g - 2$, where c is the number of branches of the core and m is the multiplicity of monomer. For EDA cored PAMAM, $c = 4$ and $m = 2$. At physiological pH 7.4, most of the primary amines are protonated, and by pH 4 all of the tertiary amines are also protonated.[1] The protonation level of the PAMAM can be altered by changing the solution pH, which in turn affects significantly the structure of PAMAM dendrimer. The size of the dendrimers also depends on the solvent quality, but there is disagreement concerning the magnitude and sign.[2,3] Small-angle neutron scattering experiments (SANS) in dilute solutions of $D(CD_2)_mOD$ (with $m = 0, 1, 2, 4$) show[2] that with decreasing solvent quality the radius of gyration of generations 5 and 8 PAMAM dendrimer decreases by approximately 10%. However, other experiments contradict these findings. Recently, Nisato et al.[4] have studied the effect of ionic strength and pH on the conformational change of generation 8 PAMAM dendrimer in D_2O using small-angle neutron scattering. They observed that the size of the generation 8 PAMAM dendrimer is insensitive to the variations of pH. This is also contrary to the predictions of Monte Carlo (MC) simulation studies by Welch and Muthukumar,[5] who predicted almost a 180% increase in dendrimer size as the ionic concentration and pH of the solvent are increased. Similarly, a Brownian dynamics study by Murat and Grest[6] revealed an increase in internal segment density when the dendrimer and solvent interactions are less favorable, which results in a 45%−48% decrease of the size of the PAMAM structures.

Table 1. Number of Atoms as Well as Primary and Tertiary Nitrogens in Different Generation PAMAM Dendrimer for Fully Atomistic Model

generation	no. of atoms	no. of primary nitrogens	no. of tertiary nitrogens
0	84	4	2
1	228	8	6
2	516	16	14
3	1092	32	30
4	2244	64	62
5	4548	128	126
6	9156	256	254
7	18372	512	510
8	36804	1024	1022
9	73668	2048	2046
10	147396	4096	4094
11	294852	8192	8190

A major goal of this paper is to investigate systematically the behavior of PAMAM dendrimer at various protonation levels in a good solvent. A few simulations[7] have been reported on the effect of protonation, but these simulations were performed in the absence of explicit solvent as well as counterions. Such approximations may lead to unphysical results in the size and shape of the dendrimer. Also, the presence of solvent as well and counterions may significantly modify the end-group distribution within the dendrimer. In this paper we study systematically the effect of different levels of protonation in a polar solvent (water) on the structure of the dendrimer and more specifically their effect on the end-group distributions.

Some applications of dendrimers require interior voids to accommodate guest molecules for guest−host applications. The size of the internal cavities can be large

† Present address: Department of Physics, Indian Institute of Science, Bangalore, India 560012.

‡ Present address: Department of Chemical Engineering, Texas A&M University, College Station, Texas 77845-3122.

* To whom all correspondence should be addressed: e-mail wag@wag.caltech.edu.

10.1021/ma049168l CCC: $30.25
Published on Web 01/13/2005

enough to accommodate relatively big molecules such as dye Bengal Rose.[8,9] On the other hand, very little information is available on the internal structures and availability of inner cavities for PAMAM dendrimer at various solvent conditions. In this study we obtain detailed structural information about the interior of G4−G6 PAMAM dendrimers and provide a quantitative estimate of the available space inside. Several recent experiments[10−13] show that PAMAM dendrimers can form complexes with metal ions and those complexes can be used to produce metal nanoparticles upon reduction of the dendrimer−metal complexes.[14] However, taking into consideration the conventional binding mode of Cu(II) with the primary and tertiary amines fails to explain the uptake of metal ions at all Cu(II)−dendrimer loadings. To explain the enhanced uptake of Cu(II) ions at some loadings, we do a systematic investigation of the extent of water binding inside PAMAM dendrimer at various pH conditions. Our results on the number of water molecules trapped inside the PAMAM dendrimer correctly explain the extent of binding of Cu(II) ions in the recent experiment on aqueous solution of PAMAM and Cu(II) ions.[15] The results from our simulation studies provide a different binding mode for the Cu(II) ions, which helps explain the experimental results.

2. Simulation Methods

To mimic the targeted pH conditions, we carried out simulations at three protonation levels: (i) high pH: No protonation (pH > 12); (ii) intermediate or neutral pH: all the primary amines (64 for G4, 128 for G5, and 256 for G6) are protonated, but none of the tertiary amines (pH ∼ 7); (iii) low pH: all the primary amines and tertiary amines (62 for G4, 126 for G5, and 254 for G6) are protonated (pH < 4). This is the same range followed in the work by Baker and co-workers.[7] Not reported here are simulations we carried for other protonation levels to mimic the continuous variation in pH from high to low. The results of those studies will be published elsewhere[16] where we elucidate the protonation mechanisms in PAMAM dendrimer. Here, we present the results of our simulation studies on G4−G6 dendrimers at high, intermediate, and low pH in explicit water in the presence of counterions.

We generated the initial 3-dimensional atomistic structures of PAMAM dendrimers using the CCBB Monte Carlo method.[17,18] The structures generated were then subjected to conjugate gradient optimization to obtain lower energy configurations. We further annealed the minimized structures at very high temperature and cooled to room temperature. Then 200−400 ps of dynamics was performed at room temperature in the absence of explicit solvent. The final dynamic structure after 200−400 ps runs was protonated at various levels. For neutral and low pH cases Cl^- counterions were added to bring charge neutrality, resulting in a number of counterions present in the system that varies with the degree of protonation. The initial positions of the Cl^- ions were ∼3.8 Å from the primary and tertiary amine sites for neutral and low pH cases, respectively.

We used the F3C model for water since it gives satisfactory properties of bulk water at various temperatures.[19] We started with a preequilibrated box of water, which was copied and repeated, in all three spatial directions to create a box sufficiently large to contain the dendrimer. This complex was then immersed in the solvent box while deleted waters that overlap the dendrimer or counterion atoms. The box was selected to be large enough that the distance between the wall of the box and the closest atom of dendrimer was 10 Å in each direction. Since the size of the dendrimer increases in going from G4 to G6, the number of waters in a 10 Å thick water layer surrounding the dendrimer also increases. The resulting number of atoms in the simulation box is given in Table 2. After constructing the dendrimer inside the solvent box, an additional 100−200 ps of MD was performed to equilibrate the system before collecting data.

Table 2. Details of the Simulation Parameters

generation	pH	no. of atoms	no. of waters	dendrimer charge	no. of Cl^-
4	high	2244	5083	0	0
	neutral	2308	5301	64	64
	low	2370	5297	126	126
5	high	4548	9406	0	0
	neutral	4676	9374	128	128
	low	4802	12977	254	254
6	high	9156	19525	0	0
	neutral	9412	20294	256	256
	low	9666	20272	510	510

We then carried out MD simulations at 300 K for generations 4−6 in explicit water at various protonation levels. These simulations employed the Dreiding force fields[20] to describe the interactions.

The partial charges on the atoms were derived using the charge equilibration (QEq) method.[21] First, we evaluated the QEq charges for the ethylenediamine (EDA) core as a neutral molecule using generation 0, i.e., with all four terminal H atoms replaced by four monomers of PAMAM dendrimer. Then, we evaluated the QEq charges for the full monomer of PAMAM, with all three H atoms replaced by three monomers of PAMAM and required charge neutrality. Finally, we evaluated the QEq charges for the terminal PAMAM monomers, with the two terminal H atoms kept as H and the other H by a monomer of PAMAM dendrimer. These charges for the terminal PAMAM monomer were then scaled to be neutral and used for the terminal generation. This procedure ensures that each generation is neutral. In the case of intermediate pH where all primary amines are protonated, we found that the change of atomic charges is quite localized; therefore, it is sufficient to recalculate only their charges on terminal monomers. However, for the low-pH case when both primary and tertiary amines are protonated the charge was distributed to the added proton only for the tertiary proton site. We also calculated the Qeq charges over all atoms of the dendrimer for G4−G5 at low pH and found out that structural properties remain unchanged for the above two charge schemes.

To evaluate the nonbonded interactions (Coulomb and van der Waals), we used the cell multipole method (CMM)[22] with appropriate level which resulted in an average of 10−15 particles per leaf cell. To enhance the speed of simulation, we performed simulations for nonperiodic systems; i.e., the PAMAM is immersed in a spherical droplet of water (10 Å water layer corresponding to 3−4 solvation layers around dendrimer). All calculations were carried out with the MPSim program.[23] The Verlet equations of motion were integrated using an integration step of 1 fs. A Nose−Hoover type thermostat with a relaxation time of 0.1 ps was used to control the temperature. The simulations were con-

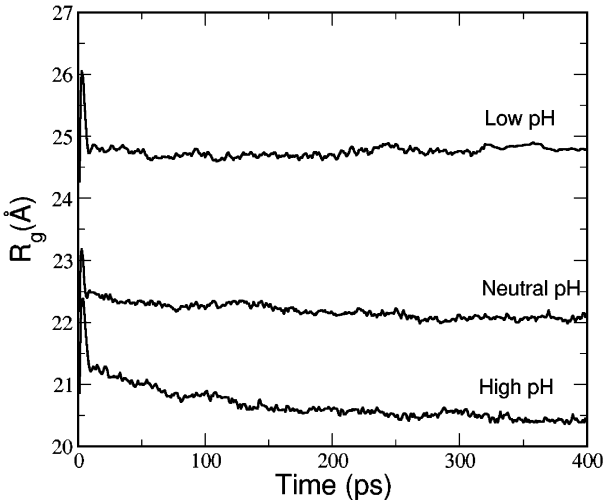

Figure 1. Time evolution of the radius of gyration (R_g) of the G5 PAMAM dendrimer at various solvent conditions.

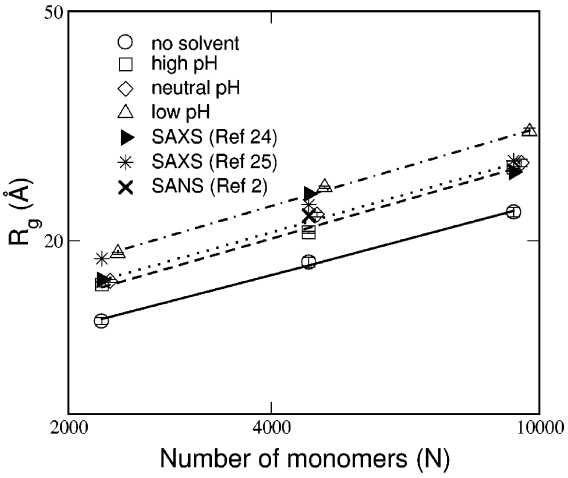

Figure 2. Radius of gyration as a function of number of monomers. For comparison, we also plot the experimental R_g from three different sources. The lines are best power law fit to the data and has the form $R_g = 1.45 + 1.06N^{0.33}$ for the case of no solvent; $R_g = -0.18 + 1.28N^{0.33}$ for the case of high pH; $R_g = 0.15 + 1.29N^{0.33}$ for the case of neutral pH; $R_g = -0.62 + 1.48N^{0.33}$ for the case of low pH. The fits indicate that at various solvent conditions radius of gyration follow same scaling relationship.

ducted at $T = 300$ K. The lengths of simulations are 400 ps (200 ps for equilibration and an additional 200 ps for data collection). These simulation times proved to be sufficient to obtain equilibrium properties as seen from the time evolution of the total energy of the system as well as the radius of gyration of the dendrimer (see Figure 1). We saved snapshots for every 0.5 ps interval in the simulations and used these configurations to determine the average properties at $T = 300$ K. The next section presents the results.

3. Results

To characterize the structure and properties of dendrimers as a function of generation at various pH conditions, we chose the following quantities: radius of gyration, shape tensor, monomer density distribution, molecular surface area, end-group distribution, solvent accessible surface, molecular volume, and spatial arrangement of branch points. To compare with the recent SANS experiments, we computed the single particle form factors at various simulation conditions. We have also studied the penetration of water inside dendrimer by computing the number of waters inside the dendrimer as a function of the distance form the center-of-mass of the dendrimer.

3.1. Size and Shape. A quantitative estimate of the dendrimer shape and size can be described by the mean-square radius of gyration $\langle R_g^2 \rangle$ and shape tensor of the individual chain. For a dendrimer with N atoms the mean-square radius of gyration is given by

$$\langle R_g^2 \rangle = \frac{1}{M} \langle [\sum_{i=1}^{N} m_i |r_i - R|^2] \rangle \qquad (1)$$

where R is the center-of-mass of the dendrimer, r_i and m_i are the position and mass of the ith atom, and M is the total mass of the dendrimer. Figure 2 shows the radius of gyration R_g as a function of number of monomers for various dendrimer generations at different protonation levels. For comparison, we also show the available experimental values for lower generations dendrimer obtained from small angles X-ray scattering (SAXS)[24,25] and SANS experiments.[2] The values of R_g obtained from our simulations along with the experimental values are also tabulated in Table 3.

- At high pH when there is no protonation, just the presence of a good solvent like water increases the size of the dendrimer by almost 10−15%. This trend is similar in all the generations reported in this paper.
- At neutral pH when all the primary amines are protonated there is no significant change in the dendrimer size as it is evident from very small increase in radius of gyration.
- As the pH is lowered further, eventually all the tertiary amines are also protonated, and at that protonation level we see almost 30−40% increase in radius of gyration compared to the case when no solvent is present.

These observations are consistent with recent experimental findings[2] which report the effect of varying solvent quality on the size of generation 5 and 8 PAMAM dendrimers. Using holographic relaxation spectroscopy (HRS), Stechmesser et al.[26] studied the size of various generation PAMAM dendrimer under varying solvent conditions. They reported a significant swelling of dendrimer in good solvents for larger generations ($G > 4$). Our simulation results are consistent with their experimental findings. However, this contradicts the experimental findings on generation 8 PAMAM dendrimer by Nisato et al.[4] They studied the behavior of G8 PAMAM dendrimer in D_2O at various pH levels using SANS and found that the dendrimer size is essentially independent of the ionic strength of the solvent.

In the presence of a polar solvent like water, we find significant penetration of water throughout the interior of the dendrimer, which causes the dendrimer structure to swell. This results from the favorable interaction of the solvent with the primary and tertiary amines. Both the excluded-volume interactions and the Coulombic repulsions between the protonated primary and tertiary amines give rise to the dramatic increase in R_g at various protonation levels. The presence of counterions also increases the swelling. Depending on the degree of protonation, a significant portion of the counterions

Table 3. Radius of Gyration R_g (Å) for EDA Cored PAMAM Dendrimers at Various Solvent Conditions[a]

									experiment		
	no solvent		high pH		neutral pH		low pH		SAXS		SANS
generation	R_g	R_N	R_g	R_N	R_g	R_N	R_g	R_N	ref 24	ref 25	ref 2
4	14.50 ± 0.28	16.81 ± 0.32	16.78 ± 0.15	18.49 ± 0.22	17.01 ± 0.1	18.84 ± 0.12	19.01 ± 0.08	21.2 ± 0.15	17.1	18.60	
5	18.34 ± 0.37	20.26 ± 0.68	20.67 ± 0.09	22.71 ± 0.47	22.19 ± 0.14	24.43 ± 0.07	24.76 ± 0.14	27.38 ± 0.18	24.1	23.07	22.1
6	22.40 ± 0.42	24.67 ± 0.49	26.76 ± 0.11	28.75 ± 0.20	27.28 ± 0.39	30.24 ± 0.45	30.89 ± 0.41	34.08 ± 0.39	26.3	27.50	

[a] R_N is the radius of gyration considering only the location of the primary nitrogens. For comparison, we also give the experimental values obtained through SAXS and SANS experiments. The experiments were performed in methanol solution.

Table 4. Number of Primary Nitrogens Located at the Periphery (Surface) of the Molecules at Various Solvent Conditions; Shown Are Also the Percentages in Brackets; Numbers of Cl^- That Are Distributed in the Interior of the Molecules Are Also Given for Neutral and Low pH

				no. of inner Cl^-	
generation	high pH	neutral pH	low pH	neutral pH	low pH
4	37 (57%)	41 (64%)	45 (70%)	10 (15%)	38 (30%)
5	48 (37%)	75 (59%)	83 (65%)	22 (17%)	38 (15%)
6	115 (44%)	152 (59%)	143 (55%)	63 (25%)	193 (38%)

condense within the dendrimer, residing very close to the protonated sites (see Table 4), with some solvated by the water. As the protonation level increases, there are more counterions inside dendrimer and the dendrimer swells more at higher protonation levels.

Figure 2 plots R_g as a function of number of monomers in the dendrimer using a log−log scale. The lines are the best fit to a power law dependence with exponents ~0.33. This scaling law holds for various solvent conditions as has been observed in HRS studies on PAMAM dendrimer in water, methanol, and butanol.[26] This scaling exponent is in excellent agreement with the recent SAXS results on PAMAM dendrimers up to generation 8[25] which find an exponent of 0.33. SANS studies on poly(benzyl ether) dendrimers[27] also indicated an exponent of 0.33. Murat and Grest[6] predicted a scaling exponent of 0.33 based on Brownian dynamics simulations on model dendrimers under varying solvent conditions. This scaling exponent indicates a compact space-filling object under various solvent conditions. To compare our simulation results with those of Welch and Muthukumar,[5] we also calculate the effective Debye length in our simulations. The effective Debye radius κ^{-1} is calculated using the following:

$$\kappa^2 = 4\pi l_B \sum_i c_i {z_i}^2 \qquad (2)$$

Here c_i and z_i are the concentration and valence of the ith ion. l_B is the Bjerrum length in water at 300 K, which is taken to be 7.1 Å. The salt concentration in our simulation corresponds to a Debye length in the range 3−4 Å (4.3 Å for neutral pH and 3.6 Å for low pH for simulation conditions for G5), which represents the case of high salt concentration. Welch and Muthukumar,[5] on the other hand, report simulations with Debye length ranging from 3 to 300 Å. At larger Debye length (corresponding to very low salt concentration) due to low electrostatics screening dendrimer structure swells more, leading to larger increase in R_g in their study. Attaining such low salt concentration or larger Debye radius will require inclusion of very large number of water molecules in the simulation, which will require much more computational time.

To study the change in dendrimer conformations as a function of solution pH, we have calculated the shape of the dendrimer at various solvent conditions. The shape tensor describing the mass distribution is given by[28]

$$G_{mn} = \frac{1}{M}[\sum_i^N m_i(r_{mi} - R_m)(r_{ni} - R_n)] \qquad m, n = x, y, z \qquad (3)$$

The three eigenvalues of the shape tensor **G,** I_z, I_y, and I_x (in descending order), are the principal moments of the equivalent ellipsoid. The sum of these eigenvalues is an invariant of **G,** giving $\langle {R_g}^2 \rangle$. The ratio of these three principal moments is a measure of asphericity (minor−major axes ratio) of the shape ellipsoid of the dendrimer.

The shape of the dendrimer can be assessed from the average values of the ratio of three principal moments of inertia of the molecules. In Figure 3, we plot the average ratios for different generation dendrimers at various solvent conditions. In the presence of a good solvent (water) the ratios of the principal moment of inertia decreases and approaches to unity. This indicates that the favorable interactions with the solvent make the shape of the G4−G6 dendrimer more spherical compared to the case with no solvent. In the presence of good solvent the branches are more stretched (see

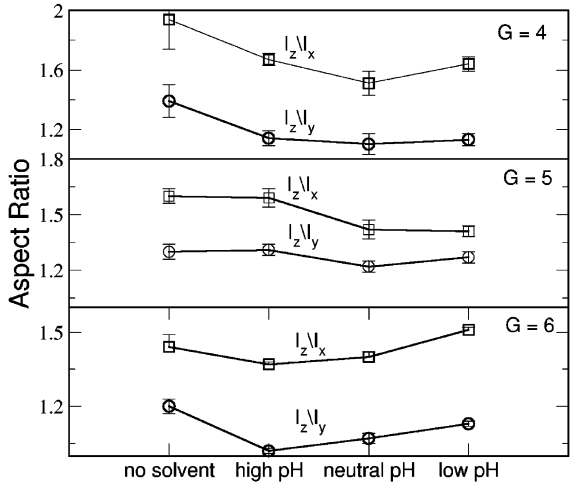

Figure 3. Moment of inertia aspect ratios for G4−G6 PAMAM dendrimer at various solvent conditions ($I_z > I_y > I_x$). These values were averaged from snapshots every 0.5 ps in the dynamics (after equilibration). The solid line is only to guide the eye.

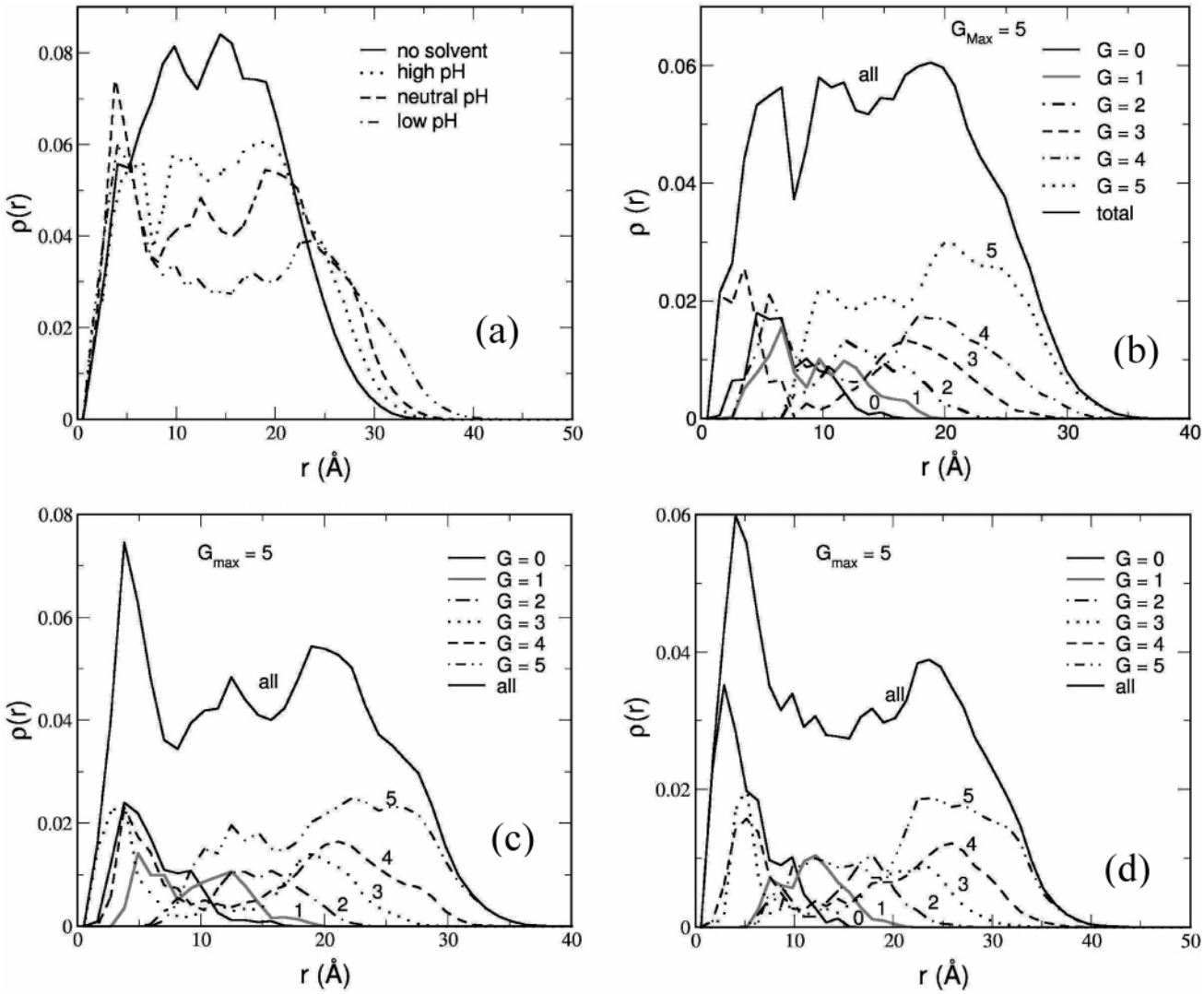

Figure 4. (a) Radial monomer densities for generation 5 PAMAM dendrimer at various solvent conditions. (b) In explicit water. We have also shown the contributions coming from various subgenerations. Comparison of the density profiles for generation 5 PAMAM dendrimer at various protonation levels. (c) All the primary nitrogens are protonated (neutral pH). (d) All the primary and tertiary nitrogens are protonated (low pH).

Figures 6 in the branch point distribution section), giving rise to greater uniformity in the spatial distribution of various branches and thus a greater sphericity. Similar behavior is also observed in the Monte Carlo simulation of star polymers in good solvent.[29,30] At neutral or low pH electrostatic repulsion between the primary and tertiary amines leads to further stretching of branches. The solvation of the dendrimers (high pH) results in more spherical overall structures for G4 through G6, and neutral pH conditions leads to further increase in sphericity for G4 and G5. Low-pH conditions which led to further increase in size and stretching consistently lead to less spherical shapes compared to high- and neutral-pH cases. This effect is more pronounced in G6; in this case asphericity is larger than even from the no solvent condition.

3.2. Radial Monomer Density Profiles. The average radial monomer density $\rho(r)$ can be defined by counting the number of atoms whose centers-of-mass are located within the spherical shell of radius r and thickness Δr. Hence, the integration over r yields the total number of atoms $N(R)$ as

$$N(R) = 4\pi \int_0^R r^2 \rho(r)\, \mathrm{d}r \qquad (4)$$

Figure 4 plots the radial monomer density for G5 PAMAM dendrimer in water at varying pH conditions. For comparison, we also show the density profile for the case with no solvent present. We find that in the presence of solvent (whether neutral or low pH) the total density shows a minimum at around 10 Å away from the core. A secondary peak near the periphery of the molecules follows this minimum. This indicates that the core regions become denser compared to the middle of the dendrimer, which is fairly hollow. This picture is consistent with the previous Monte Carlo as well theoretical prediction by Muthukumar and co-workers.[5] This location of the minimum increases with the increase in generations. Also, we note that this increase in density at the core comes from the density of only the inner generations. The outermost generation does not contribute to this density. Because of this hollowness at the middle regions of the dendrimer, a significant number of waters may penetrate to the middle of the dendrimer. The water density profiles shown in Figure 7a as well as the number of water inside dendrimer shown in Figure 8 support this picture. As the size of the dendrimers increases due to the swelling, the density profile extends more radially outward compared

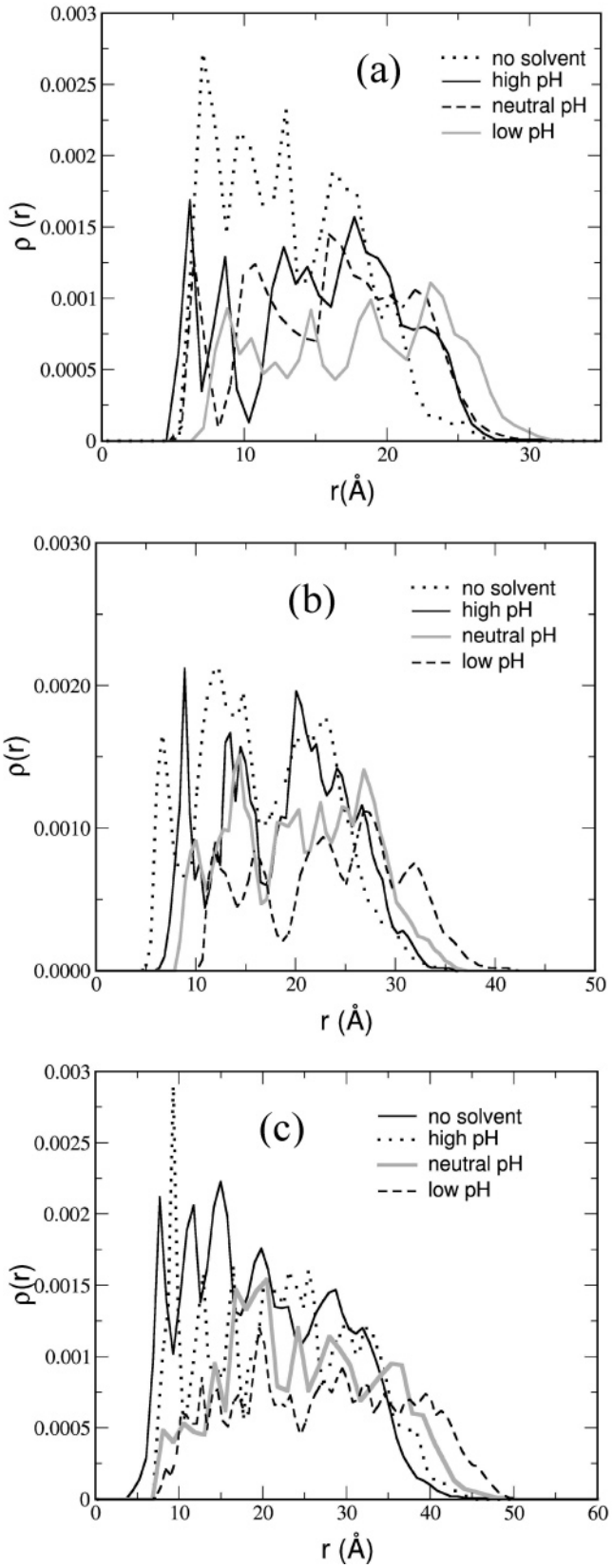

Figure 5. Radial monomer density distribution of the primary nitrogens at various solvent conditions for (a) G4, (b) G5, and (c) G6 PAMAM dendrimer.

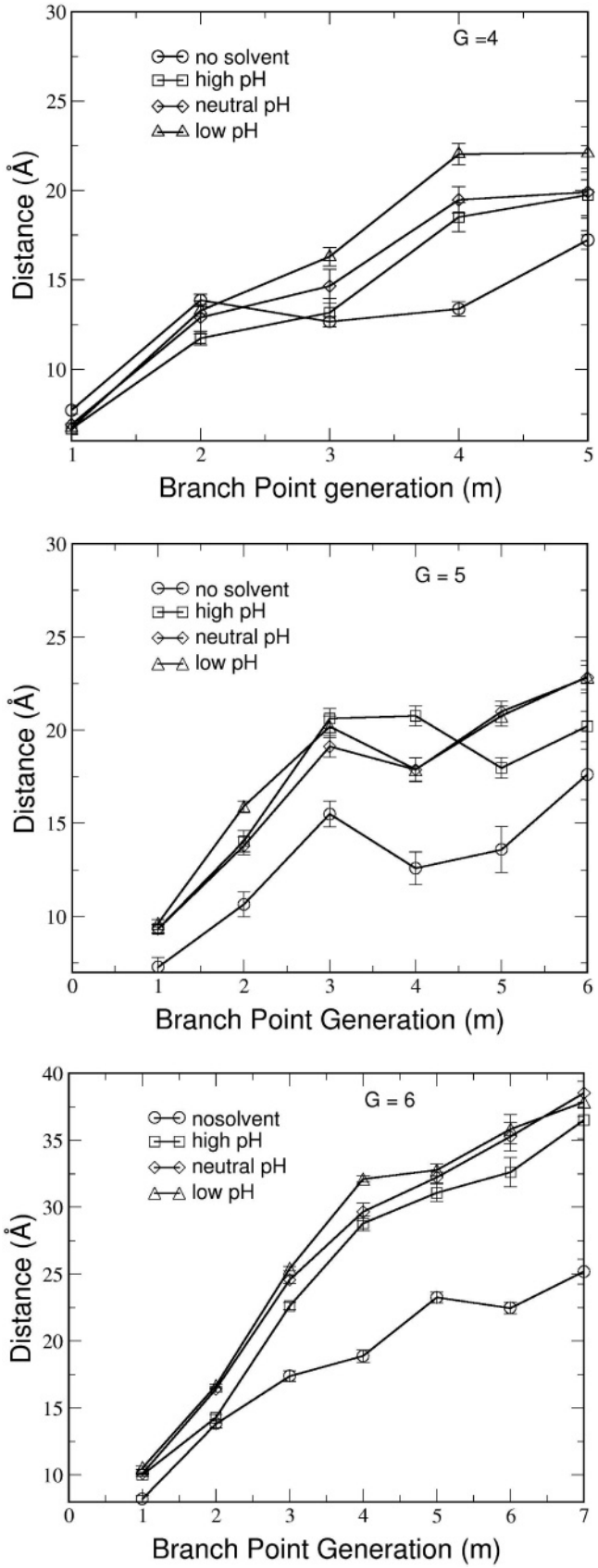

Figure 6. Branch point distance distributions functions. Distance is measured from the center-of-mass of the core to the branch point for G4−G6 PAMAM dendrimer

to the no solvent case. This behavior is more pronounced at higher protonation level when the pH is low. The contributions of the monomers belonging to consecutive generations are also shown. Compared to the no solvent case, we see that the presence of a good solvent like water reduces significantly the back-folding of the outer generations. As a result, the contributions coming from each subgenerations to the total density gradually

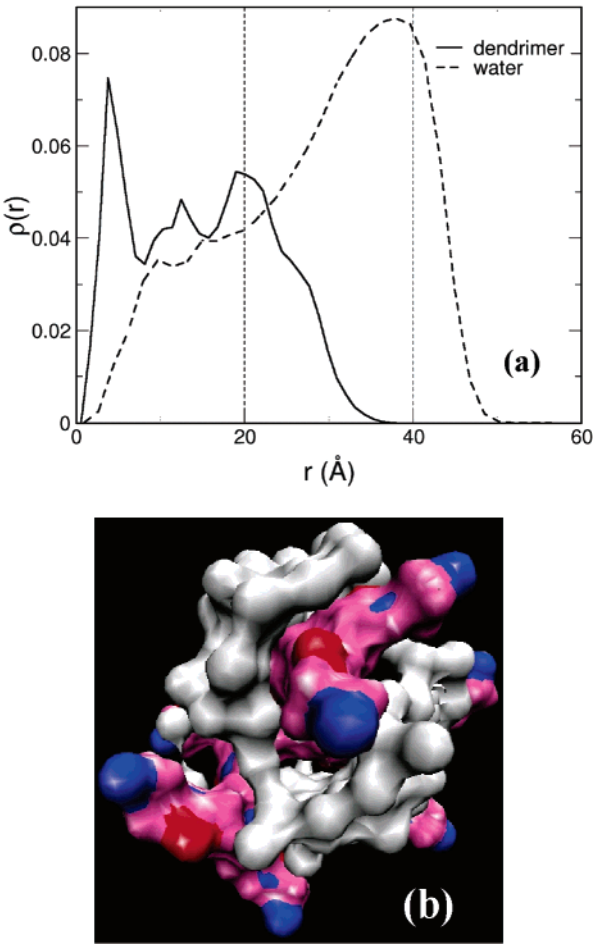

Figure 7. (a) Degree of water penetration in generation 5 PAMAM dendrimer when all the primary amines are protonated. (b) Structure of innermost water layer for generation 5 PAMAM at low pH. The water surface is shown in gray color. Surfaces of various dendrimer atoms are shown in RGB CPK color: blue for nitrogen, red for oxygen, mauve for carbon, and white for hydrogen.

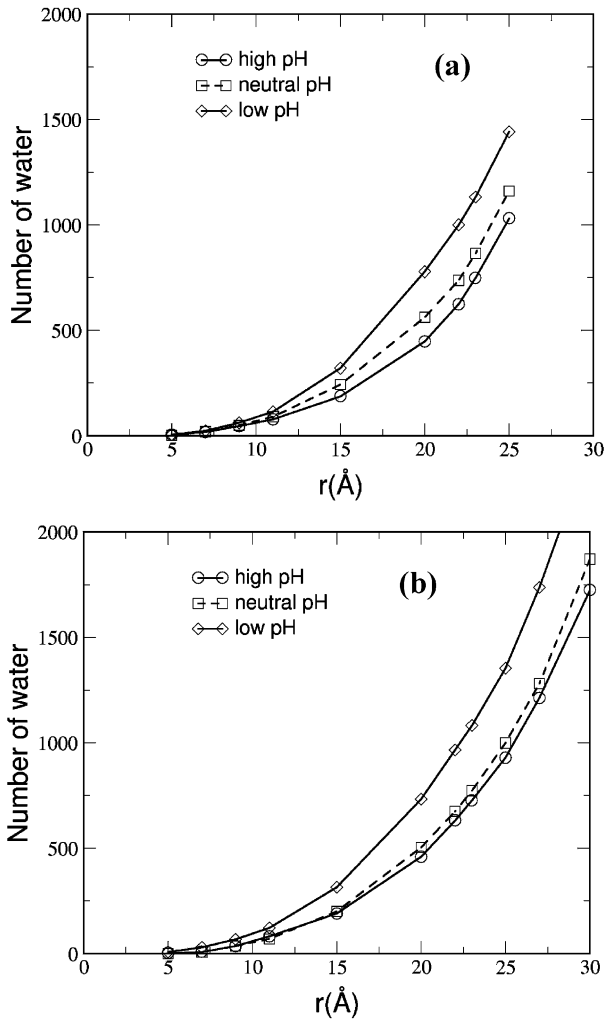

Figure 8. Number of water inside (a) generation 5 and (b) generation 6 PAMAM dendrimer as a function of distance from the center of core at various pH levels

decrease near the core of the dendrimer. Consequently, the total monomer density shows a minimum at the core and gradually increases with a maximum at some distance from the core, which roughly corresponds to its radius of gyration. Beyond that it decays monotonically.

3.3. Terminal Amine Group Distribution. Many of the applications of the dendrimer rely heavily on the availability of the functional end groups as well as their distribution over the molecule. Several experimental and computational studies indicate that there is significant back-folding of the outer subgeneration throughout the interior of the molecules.

A recent SANS experiment on G7 PAMAM dendrimer[31] was interpreted to indicate that the terminal units are located at the periphery of the molecules. Their argument was based on the observations that the radius of gyration of the terminal groups (R_N) was larger than the R_g of the entire dendrimer. However, our earlier paper[17] showed that this is not an accurate measure since distribution functions with $R_N \geq R_g$ can be achieved even when most of the end groups are located within the interior of the dendrimer molecules. Lyulin et al.[32,33] also came to the same conclusion based on their Brownian dynamics simulations. On the other hand, on the basis of rotational-echo-double-resonance (REDOR) of the Frechet-type dendrimers, Wooley et al.[34] showed that even in the solid state there is significant back-folding with the radial monomer density decaying monotonically with the increasing distance from the center-of-mass of the molecules. Measurements of spin−lattice relaxation in polyaryl dendrimers with a paramagnetic core[35] also reveal that the end groups are close to the core of the molecules. Thus, there remains a controversy over whether the end groups are located at the periphery of the molecule or located inside the dendrimer molecule due to substantial folding back of the end groups.

To probe this issue, we calculated the distribution of terminal nitrogens for various generations, as shown in Figure 5. We see that the end groups of a given dendrimer are sufficiently flexible to interpenetrate the whole molecule. In particular, the end groups of the higher generations even come very close to the core of the molecule. Earlier, we demonstrated[17] that in the case of no solvent the terminal groups are distributed throughout the interior of the molecule. We see similar behavior in a good solvent in various pH levels. However, the location of the maximum terminal density gradually shifts toward the periphery with the increase in protonation level. Also, the density profile exhibits multiple peaks for all generations at all pH levels. As the pH is lowered so that the tertiary amines get

protonated, the density profile of the primary nitrogen atoms are pushed further toward the periphery of the molecule due to the new electrostatics interactions that prevent back-folding of the primary (terminal) nitrogen atoms. To obtain a quantitative measure of the degree of back-folding, Table 4 shows the number of primary nitrogens at the periphery of the dendrimer molecules for various generation PAMAM dendrimer at various pH levels. For G5 at high pH only 37% of the primary amines are located at the outer periphery of the molecules. As the solution pH is lowered to protonate the primary and tertiary amines, almost 65% of the primary amines are now on the surface. We observed similar trends for G4 and G6 as well.

3.4. Branch Point Distribution. The distributions of the end groups are highly dependent on how the different branch points ("spacers") are arranged in space. The overall shape of the dendrimer may also depend on the arrangements of various branches within the molecule. The de Gennes and Hervet paper[36] assumed that the spacers near the center of the molecules behave like flexible coils or less stretched, while those at the outer regions are elongated. To see how the presence of solvent as well as various solvent conditions affects the distribution of branch points, we calculated the branch point distance from the center of core of the dendrimer as a function of the branch point generations. This helps us understand how the spacers or the branch points are spatially arranged. Figure 6 shows the branch point distance from the center of core of the dendrimer as a function of the branch point generations for G4−G6 PAMAM dendrimer at various solvent conditions. In all the cases the presence of a good solvent helps to stretch out the successive branch points radially. With decreased pH, we see that the various branch points are pushed out even further causing a greater expansion of various branches. The greater expansion of various branches helps to achieve favorable interaction with the solvent as well as higher conformational entropy. This allows various branches to accommodate the interatomic repulsion without excessive overcrowding at the interior.

This observation is consistent with the relative increase in R_g as well as the increasingly spherical character with lower solvent pH. Similar behavior has been reported for regular star polymers in a good solvent. Because of this increase in branch point distance from the center of the molecule, there is a drop in the density in the middle of the dendrimer as evident from the density profile shown in Figure 4. Another important feature that can be extracted from Figure 6 is that the bonds at the core are more stretched, a feature that becomes stronger for larger generations. On the other hand, the terminal branch points are the least stretched. This is consistent with our earlier observation that the core domain is denser for lower generation dendrimers in comparison to the higher generation.

3.5. Water Penetration. Because of the swelling of the dendrimer structure in the presence of good solvents, a significant part of the inner surface and volume of the dendrimer are accessible to the solvent. Consequently, we see that large number of water molecules has penetrated throughout the interior of the dendrimer. Figure 7a plots the density profile for water molecules and dendrimer for G5 PAMAM dendrimers at neutral pH. The density profiles for G4 and G6 dendrimer at various pH have similar features.

Table 5. Average Number of Water Inside Dendrimer at Various pH Levels for Different Generation PAMAM Dendrimers[a]

generations	high pH	neutral pH	low pH
4	138	201	325
5	378	524	757
6	890	1344	1731

[a] For criteria used in identifying the bound waters see the text.

Figure 8a,b also shows the number of waters as a function of distance as we go radially outward from the core of the dendrimer. We see a significant number of waters inside the dendrimer, which come within a distance of 10 Å from the core of the dendrimers. As the protonation level is increased, the dendrimer structure swells, and there is a gradual increase in the number of waters inside dendrimer for all the generations.

The structure of first solvation shell within the dendrimer is shown in Figure 7b. A quantitative estimate of the solvent penetration is given by counting the number of waters bound by the dendrimer outer surface. Because of the nonuniformity as well as asphericity of the dendrimer surface, special care must be taken to identify the bound water, as simple spherical cutoff will overestimate the numbers of waters within the dendrimer. To have an accurate estimate of the number of bound waters, we have used following criteria: We first calculated the molecular surface area (MSA) for each of the dendrimer atom using a large probe radius (6 Å). With this probe radius the generated surface of the dendrimer becomes almost spherical and smooth. Those atoms with nonzero MSA represent the surface atoms of the dendrimer. Using these surface atoms, we identify all the surface waters that are within 4 Å of the surface atoms. Next, we identify all the waters close to the inner atoms (with zero MSA), excluding all the previously defined surface waters. The number of bound waters calculated this way is listed in Table 5.

For example, for G5 at high pH we have three water/tertiary amines (378 waters for 126 tertiary amines), while this number increases to six water/tertiary amines (756 waters for 126 tertiary amines) at low pH. This significant penetration of solvent molecules inside the dendrimer structure is in agreement with the recent SANS studies on poly(benzyl ether)[27] and polycarbosilane dendrimers.[37] In these experiments the number of solvent molecules inside the dendrimer was calculated from the change in neutron scattering density. In general, a lower relative density leads to a larger solvent content inside the dendritic structure and vice versa.[27] Recent measurements of Cu(II) binding to PAMAM dendrimers show[15] that extent of Cu(II) binding exceeds that expected for specific binding by primary and tertiary amines alone. In fact, considering only the binding mode by primary and tertiary amines as proposed by Ottovani et al.[12,38] accounts for a part of the metal ion binding. But considering the binding of Cu(II) by the interior waters provides an estimate of the extent of binding that is in close agreement with the experimental observations.[15] The calculated number of waters inside dendrimer gives significant insight into the possible mechanism of Cu(II) ions binding in PAMAM dendrimer.

3.6. Solvent Accessible Molecular Surface and Volume. We have seen there is significant solvent

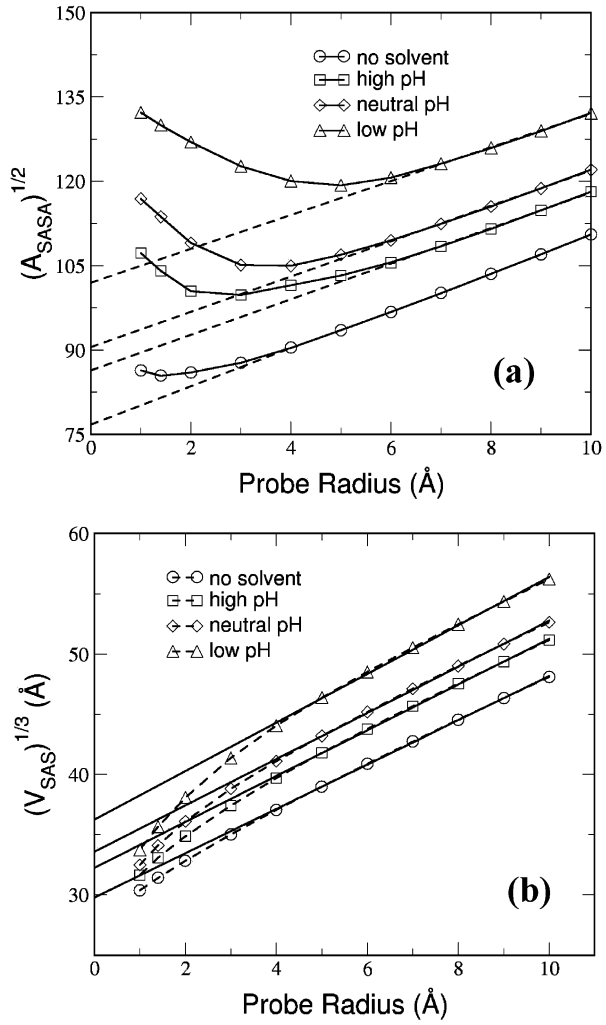

Figure 9. $\sqrt{A_{SASA}}$ (a) and $\sqrt[3]{V_{SAS}}$ (b) as a function of probe radius for generation 4 PAMAM dendrimer at various solvent and pH conditions.

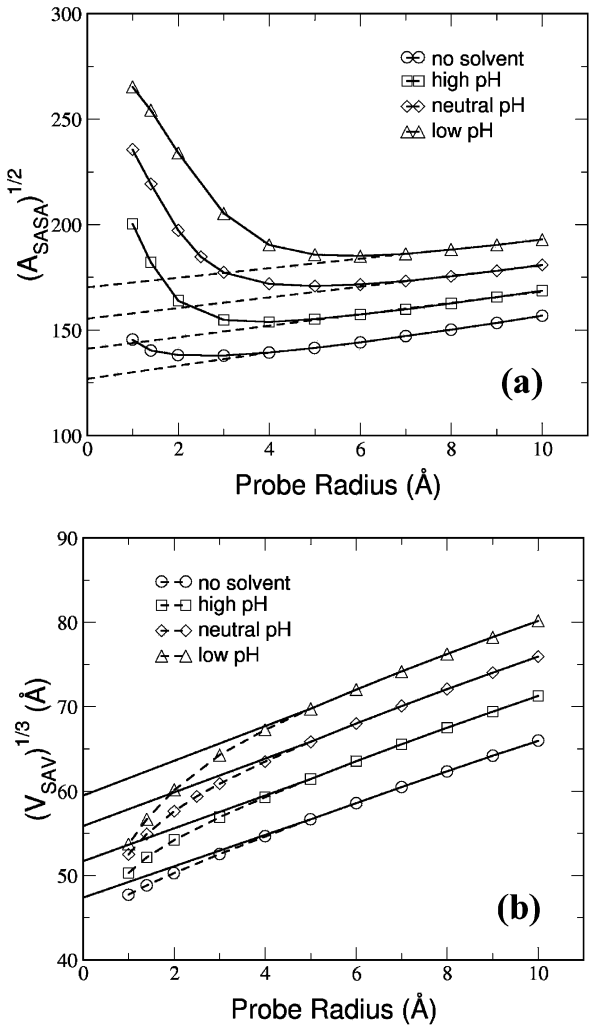

Figure 10. $\sqrt{A_{SASA}}$ (a) and $\sqrt[3]{V_{SAS}}$ (b) as a function of probe radius for generation 6 PAMAM dendrimer at various solvent and pH conditions.

penetration to the interior of the dendrimer molecules. This leads to a more open molecular structure for the dendrimers. The interaction of the dendrimers with the solvent is largely determined by its solvent accessible surface area (SASA) and solvent excluded volume. There still remains significant accessible internal surface area in a solvent-filled dendrimer. To calculate the solvent accessible surface area and volume, we assume a fused-sphere model for the solute where each sphere has radius r_i equal to the van der Waals radius of the atom it represents, r_i^{vdW} extended by the probe radius of the solute, r_p, i.e., $r_i = r_i^{vdW} + r_p$. The SASA is defined as the surface traced by the center of a spherical solvent probe as it rolls around the van der Waals spheres of the solute. For the calculation of SASA and solvent accessible volume we used analytical volume generalized Born method (AVGB) developed in the Goddard group.

Figures 9 and 10a plot $\sqrt{A_{SASA}}$ as a function of probe radius for PAMAM dendrimers for generations 4 and 6 at various solvent conditions. The plot for G5 is qualitatively similar to those of G4 and G6 dendrimers. These plots show that the SASA increases linearly with the probe radius (except for small probe radius). For small probe radius we see deviations from the linear behavior due to the extra surface in the interior of dendrimer. We see that the available internal surface area increases with the increase in protonation level. Assuming the shape of the dendrimer to be spherical, we can estimate the exterior surface area as well as the size of the dendrimer from these plots using linear regression. The size (R_{SASA}) of the dendrimer obtained this way is given in Table 6. The difference between the calculated points and the line in Figures 9 and 10a gives the internal area of the pores and internal voids. This internal surface area is plotted as a function of generation for a probe radius of 1.4 Å in Figure 11a. The available internal surface area increases dramatically in the presence of good solvent as well as with the increase in the degree in protonation level (i.e., with the lowering of solution pH). The relative increase in the available internal surface area increases in higher generations. Table 7a gives the available internal surface area for generation 4−6 PAMAM dendrimers at various solvent conditions.

We also calculated the volume associated with the internal cavities by calculating the volume contained inside the SASA, which is called the solvent accessible volume (SAV) as a function of probe radius. For a perfect sphere devoid of internal cavities, the volume contained within the sphere's SASA is given by

$$V_{SAV} = \frac{4}{3}\pi(R + r_p)^3 \qquad (5)$$

Table 6. Sizes (Å) of Various Generations EDA Cored PAMAM Dendrimers at Various Solvent and pH Conditions Using Four Different Procedures As Discussed in Text

	high pH				neutral pH				low pH			
generation	R_{SASA}	R_{SAV}	from R_G	R_N	R_{SASA}	R_{SAV}	from R_G	R_N	R_{SASA}	R_{SAV}	from R_G	R_N
4	24.37	20.00	21.66	18.49	25.52	20.83	21.96	18.84	28.77	22.48	24.54	21.20
5	30.72	25.04	26.68	22.71	33.70	26.67	28.65	24.43	38.16	29.06	31.97	27.38
6	39.83	32.07	34.55	28.75	43.83	34.65	35.22	30.24	48.05	36.91	39.88	34.08

Figures 9 and 10b show $\sqrt[3]{V_{SAV}}$ as a function of probe radius r_p for different generations PAMAM dendrimer. For larger probe radius $\sqrt[3]{V_{SAV}}$ is linear in r_p with a slope $\sqrt[3]{4/3\pi}$. The intercept at zero probe radius leads to an estimate of the volume contained inside the dendrimer, including all internal pores and cavities. Using the limit of the line in Figures 9 and 10b for $r_p = 0$ leads to an estimate the size R_{SAV} of the dendrimer in Table 6.

The deviation of the SAV from the line in Figures 9 and 10b gives a measure of the volume contained in the internal voids and cavities. This internal void volume is plotted as a function of generation for probe radius 1.4 Å in Figure 11b. We see behavior similar to the area plot. With a decrease in solution pH, there is significant

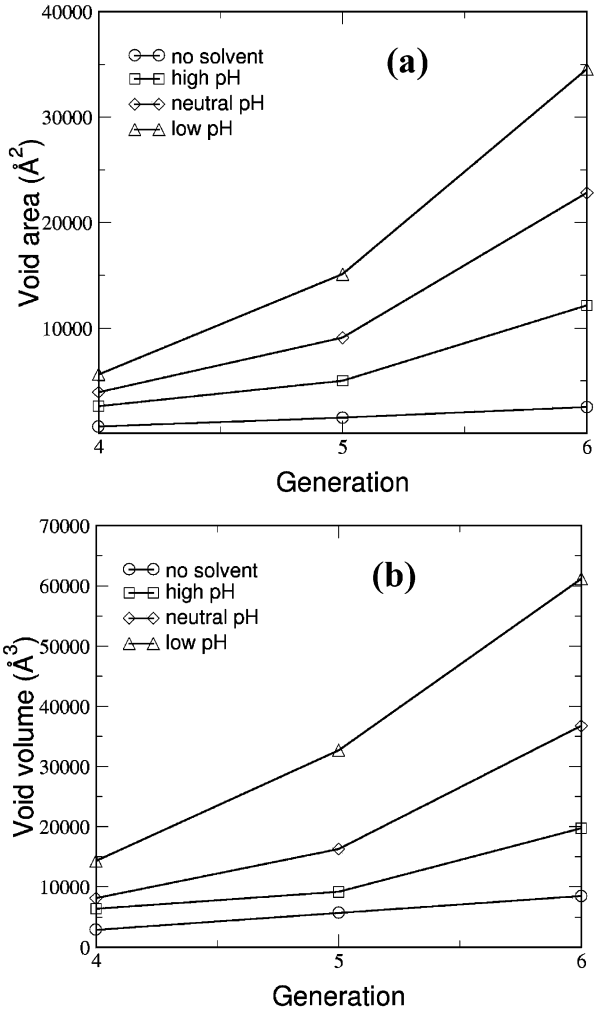

Figure 11. (a) Area and (b) volume of the internal cavities for G4−G6 PAMAM dendrimers at various solvent conditions. The area and volume have been calculated from the difference in calculated numbers and lines in figures for a probe radius of 1.4 Å. With the lowering of solution pH dendrimer structure is wide open and a single continuous channel percolates the dendrimer structure.

Table 7. Available Internal Surface Area (Å^2) and Internal Surface Volume (Å^3) for Various Generation PAMAM Dendrimers at Various Solvent Conditions[a]

generation	no solvent	high pH	neutral pH	low pH
	Internal Surface Area (Å^2)			
4	664.22	2582.70	3922.10	5621.95
5	1501.90	5015.05	9085.20	15107.32
6	2514.78	12145.56	27702.60	34551.97
	Internal Surface Volume (Å^3)			
4	2891.13	6362.57	8101.65	14290.29
5	5703.05	9157.54	16299.00	32707.00
6	8486.68	19713.79	36726.80	61191.17

[a] The area was calculated from the difference in calculated numbers and lines in figures for a probe radius of 1.4 Å.

increase in the available internal volume beyond generation 5 (Table 7b). This is consistent with the previous gene delivery experiments where a good amount of gene expression was found for dendrimer generation greater than 5.[39]

To visualize the structure of internal cavities in Figure 12, we show the solvent excluded surface area for a slice 2 Å thick passing through the center of G5 PAMAM dendrimer at various pH. At high pH we see presence of smaller pores and cavities. At neutral and low pH some of these channels open up and connect the outer surface. At this pH small molecules can diffuse in and out of the dendrimer interior. This opening up of the inner channels at lower pH will allow the dendrimer to be used as drug delivery materials. Drug can be inserted in the interior of the dendrimer at high pH and can be injected into the cell where lower pH will help open up the dendrimer structure, which in turn will allow the drug molecule to diffuse from the interior of the dendrimer molecule.

We also computed the void distribution of the inner cavities by the CASTp server at UIC.[40] This program computes the pockets and cavities present in macromolecules using alpha-shape and discrete flow methods.[41,42] The distribution of voids obtained this way has been shown in Figure 13 for the G5 PAMAM dendrimer in the absence of solvent and at low pH. The volume distribution of the cavities indicates that there exists a single big cavity, which percolates the whole dendrimer structure.

4. Structure Factor

More detailed insight about the dendrimer structure as well as direct comparison with the SANS experiment can be obtained by calculating the spherically averaged single particle form factor, $S(q)$, which is given by[43]

$$S(q) = \frac{1}{4\pi N^2}\int_0^{2\pi} d\phi \int_0^{\pi} \sin\theta \, d\theta \, |\sum_{i=1}^{N} \exp[i\vec{q}.\vec{r}_i]|^2 \quad (6)$$

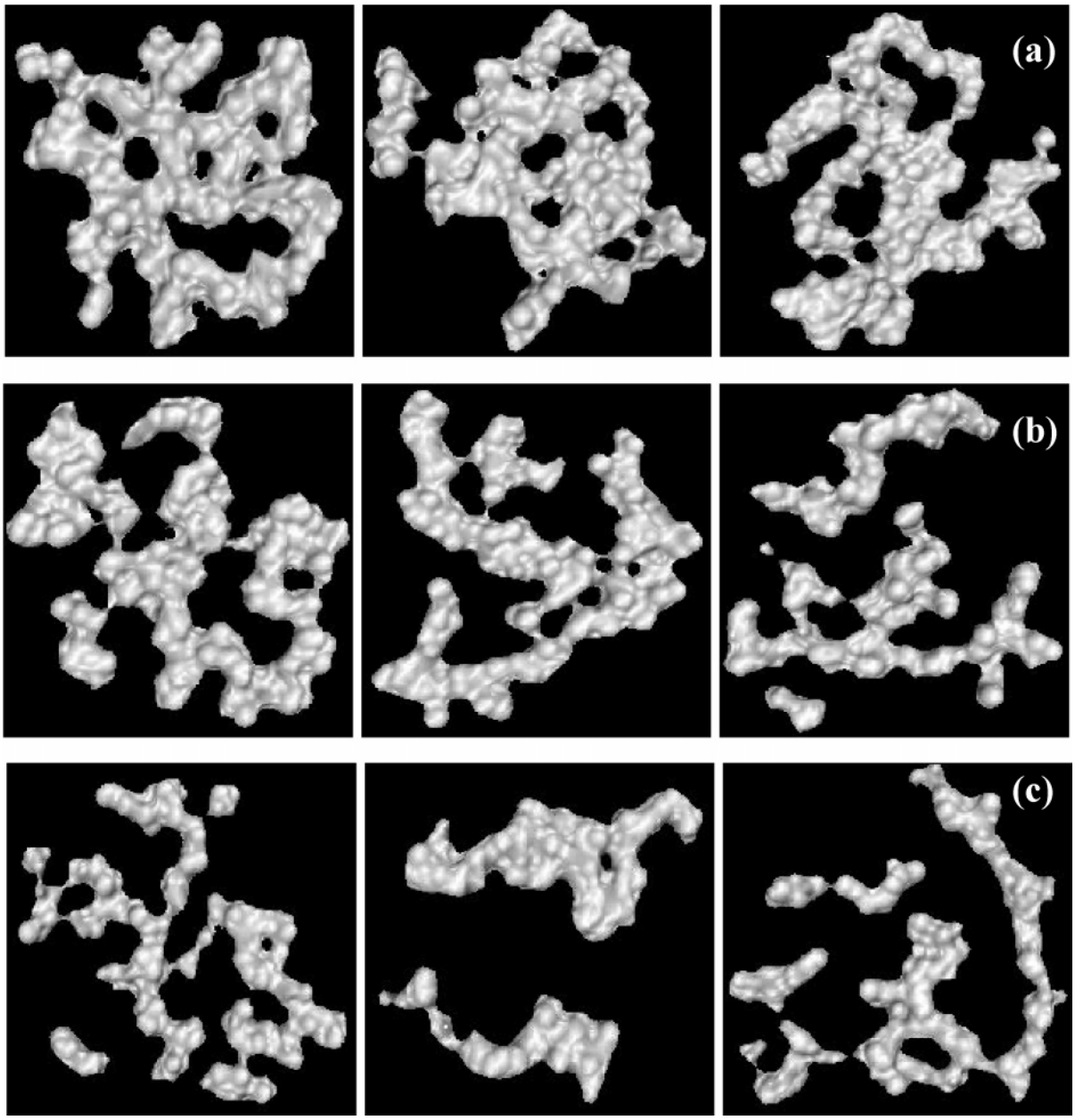

Figure 12. Solvent excluded surface area for G5 EDA cored PAMAM dendrimer at various solvent conditions: (a) high pH, (b) neutral pH, and (c) low pH. To see the interior structure, we show 2 Å thick cuts (*xy*, *xz*, and *yz*, respectively) passing through the geometric center of the dendrimer.

where

$$\vec{q} = q \sin\theta \cos\phi\hat{x} + q \sin\theta \sin\phi\hat{y} + \cos\theta\hat{z}$$

We have done the sampling for orientational averaging of scattering at intervals of 9° in both θ and φ variables. The ensemble averaging has been accomplished using 50−100 configurations spaced 1 ps apart. Figure 14 shows the Kratky plot of generation 5 and 6 PAMAM dendrimers at various solvent conditions and protonation levels. The Kratky representation helps us remove the length scale dependence and highlights the differences in the particle density distribution. Sharpening of the secondary peaks with increase protonation levels indicates that development of internal ordering inside dendrimer structure. The appearance of distinct peaks in the range $4 < qR_g < 10$ indicates that with increasing protonation level dendrimer becomes more spherical in shape. Similar behavior is also observed in the recent SANS experiment on the charged dendrimer solution.[44]

5. Conclusions

G4−6 PAMAM dendrimer have been simulated in explicit water over a range of pH conditions. Significant conformational change as well as changes in size is observed under varying solvent conditions. The presence of solvent leads to swelling the dendrimer by 33% (G5) compared to the case of no solvent. With decreasing solution pH, there is further increase in the size of the dendrimers. We find good agreement between the calculated radius of gyration and the available SAXS and SANS data. At neutral or low pH due to electrostatic repulsion between the primary and tertiary amine sites various branches are stretched out, and consequently the terminal nitrogens are pushed further toward the periphery. But still we see significant backfolding of the outer subgenerations as well as the

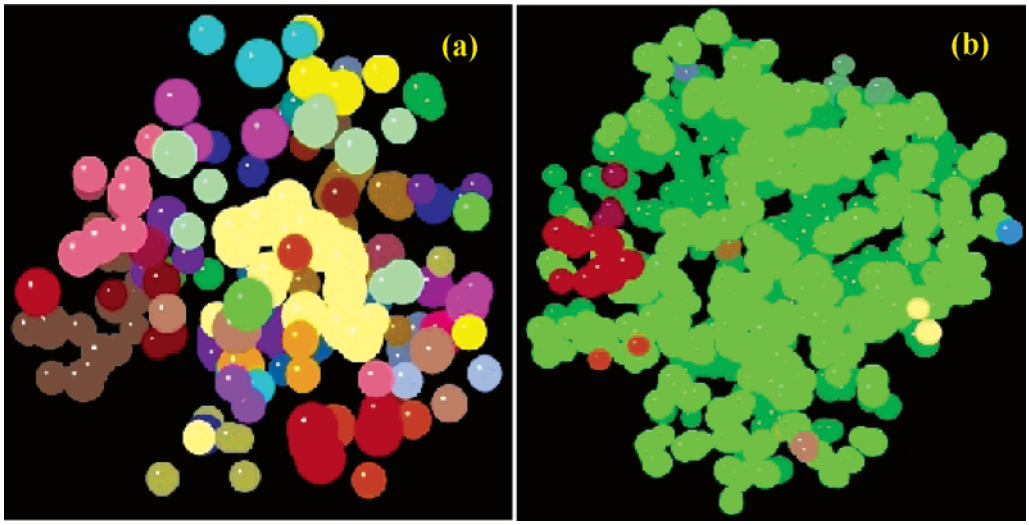

Figure 13. Structure of the inner channels and cavities for G5 dendrimer at (a) no solvent condition and (b) low pH. In the absence of solvent there exists only small pockets. At low pH apart from few small cavities we see the existence of a single continuous channel shown in green. Various other colors represent cavities of different sizes. The distribution of the cavities/channels was calculated using the CASTp server at UIC. The picture was generated using Mage software developed in Richardson's lab at Duke University.

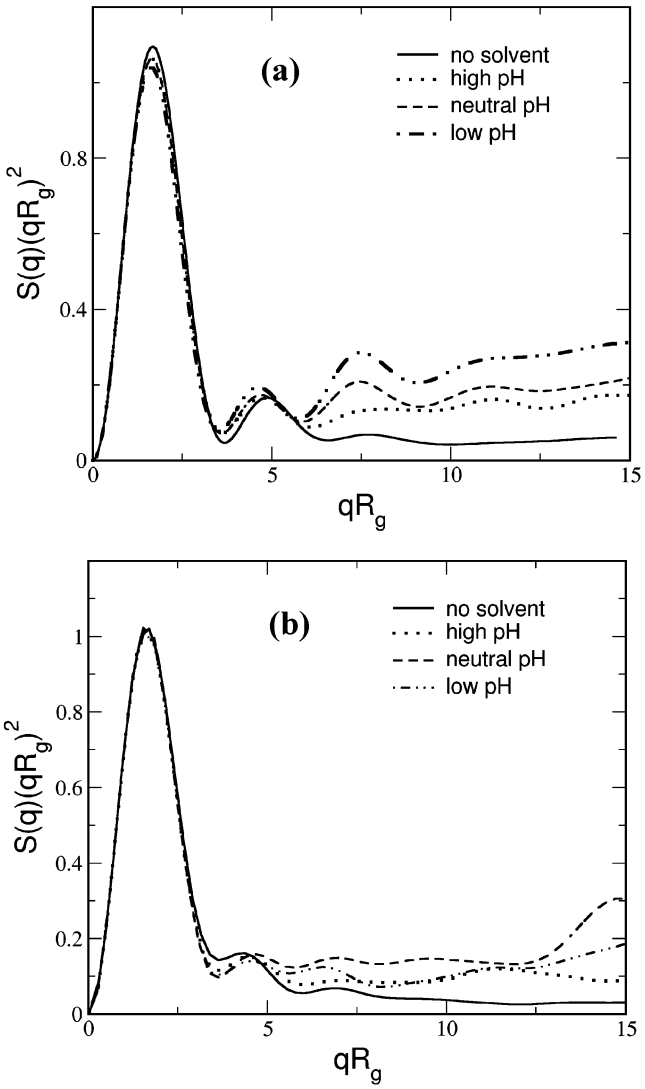

Figure 14. Kratky plots for (a) G5 and (b) G6 PAMAM dendrimer at various solvent conditions and pH levels.

terminal nitrogens. Even at low pH, when all the primary and tertiary amines are protonated, almost 40% of the primary amines are located in the interior of the dendrimer. As the solution pH is lowered, dendrimer structure become very open, and consequently there is significant penetration of solvent molecules in the interior of dendrimer molecules with ~3 water/tertiary amine for high pH and ~6 water/tertiary amines for low pH (all for G5).

Acknowledgment. We thank Dr. Mamadou Diallo for useful discussions. We thank an anonymous referee for bringing out the issue of calculating effective Debye length. This material is partly based upon work supported by, or in part by, the U.S. Army Research Laboratory and the U.S. Army Research Office under Grant DAAG55-97-1-0126 (Doug Kiserow) and completed with funding from NSF (NIRT CTS-0132002). The facilities of the MSC are also supported by grants from ARO (DURIP), ONR (DURIP), NSF, NIH, ChevronTexaco, General Motors, Seiko Epson, Asahi Kasei, and Beckman Institute.

References and Notes

(1) van Duijvenbode, R. C.; Borkovec, M.; Koper, G. J. M. *Polymer* **1998**, *39*, 2657.
(2) Topp, A.; Bauer, B. J.; Tomalia, D. A.; Amis, E. J. *Macromolecules* **1999**, *32*, 7232.
(3) Stechemesser, S.; Eimer, W. *Macromolecules* **1997**, *30*, 2204.
(4) Nisato, G.; Ivkov, R.; Amis, E. J. *Macromolecules* **2000**, *33*, 4172.
(5) Welch, P.; Muthukumar, M. *Macromolecules* **1998**, *31*, 5892.
(6) Murat, M.; Grest, G. S. *Macromolecules* **1996**, *29*, 1278.
(7) Lee, I.; Athey, B. D.; Wetzel, A. W.; Meixner, W.; Baker, J. R. *Macromolecules* **2002**, *35*, 4510.
(8) Jansen, J.; Debrabandervandenberg, E. M. M.; Meijer, E. W. *Science* **1994**, *266*, 1226.
(9) Miklis, P.; Cagin, T.; Goddard, W. A. *J. Am. Chem. Soc.* **1997**, *119*, 7458.
(10) Balogh, L.; Tomalia, D. A. *J. Am. Chem. Soc.* **1998**, *120*, 7355.
(11) Ottaviani, M. F.; Montalti, F.; Turro, N. J.; Tomalia, D. A. *J. Phys. Chem. B* **1997**, *101*, 158.
(12) Ottaviani, M. F.; Bossmann, S.; Turro, N. J.; Tomalia, D. A. *J. Am. Chem. Soc.* **1994**, *116*, 661.
(13) Diallo, M. S.; Balogh, L.; Shafagati, A.; Johnson, J. H.; Goddard, W. A.; Tomalia, D. A. *Environ. Sci. Technol.* **1999**, *33*, 820.
(14) Esumi, K. *Top. Curr. Chem.* **2003**, *227*, 31.

(15) Diallo, M. S.; Christie, S.; Swaminathan, P.; Balogh, L.; Shi, X.; Um, W.; Papelis, C.; Goddard, W. A.; Johnson, J. J. *Langmuir* **2004**, *20*, 2640.
(16) Maiti, P. K.; Lin, S. T.; Cagin, T.; Goddard, W. A. Manuscript in preparation.
(17) Maiti, P. K.; Cagin, T.; Wang, G. F.; Goddard, W. A. *Macromolecules* **2004**, *37*, 6236.
(18) Cagin, T.; Wang, G. F.; Martin, R.; Breen, N.; Goddard, W. A. *Nanotechnology* **2000**, *11*, 77.
(19) Levitt, M.; Hirshberg, M.; Sharon, R.; Laidig, K. E.; Daggett, V. *J. Phys. Chem. B* **1997**, *101*, 5051.
(20) Mayo, S. L.; Olafson, B. D.; Goddard, W. A. *J. Phys. Chem.* **1990**, *94*, 8897.
(21) Rappe, A. K.; Goddard, W. A. III *J. Phys. Chem.* **1991**, *95*, 3358.
(22) Ding, H. Q.; Karasawa, N.; Goddard, W. A. *J. Chem. Phys.* **1992**, *97*, 4309.
(23) Lim, K. T.; Brunett, S.; Iotov, M.; McClurg, R. B.; Vaidehi, N.; Dasgupta, S.; Taylor, S.; Goddard, W. A. *J. Comput. Chem.* **1997**, *18*, 501.
(24) Prosa, T. J.; Bauer, B. J.; Amis, E. J.; Tomalia, D. A.; Scherrenberg, R. J. *Polym. Sci., Part B: Polym. Phys.* **1997**, *35*, 2913.
(25) Rathgeber, S.; Monkenbusch, M.; Kreitschmann, M.; Urban, V.; Brulet, A. *J. Chem. Phys.* **2002**, *117*, 4047.
(26) Stechemesser, S.; Eimer, W. *Macromolecules* **1997**, *30*, 2204.
(27) Evmenenko, G.; Bauer, B. J.; Kleppinger, R.; Forier, B.; Dehaen, W.; Amis, E. J.; Mischenko, N.; Reynaers, H. *Macromol. Chem. Phys.* **2001**, *202*, 891.
(28) Rapaport, D. C. *The Art of Molecular Dynamics Simulation*; Cambridge University Press: New York, 1995.
(29) Forni, A.; Ganazzoli, F.; Vacatello, M. *Macromolecules* **1996**, *29*, 2994.
(30) Forni, A.; Ganazzoli, F.; Vacatello, M. *Macromolecules* **1997**, *30*, 4737.
(31) Topp, A.; Bauer, B. J.; Klimash, J. W.; Spindler, R.; Tomalia, D. A.; Amis, E. J. *Macromolecules* **1999**, *32*, 7226.
(32) Lyulin, A. V.; Davies, G. R.; Adolf, D. B. *Macromolecules* **2000**, *33*, 6899.
(33) Lyulin, A. V.; Davies, G. R.; Adolf, D. B. *Macromolecules* **2000**, *33*, 3294.
(34) Wooley, K. L.; Klug, C. A.; Tasaki, K.; Schaefer, J. *J. Am. Chem. Soc.* **1997**, *119*, 53.
(35) Gorman, C. B.; Hager, M. W.; Parkhurst, B. L.; Smith, J. C. *Macromolecules* **1998**, *31*, 815.
(36) de Gennes, P. G. H. H. *J. Phys. (Paris)* **1983**, *44*, L351.
(37) Kuklin, A. I.; Ozerin, A. N.; Islamov, A. K.; Muzafarov, A. M.; Gordeliy, V. I.; Rebrov, E. A.; Ignat'eva, G. M.; Tatarinova, E. A.; Mukhamedzyanov, R. I.; Ozerina, L. A.; Sharipov, E. Y. *J. Appl. Crystallogr.* **2003**, *36*, 679.
(38) Ottaviani, M. F.; Valluzzi, R.; Balogh, L. *Macromolecules* **2002**, *35*, 5105.
(39) Haensler, J.; Szoka, F. C. *Bioconjugate Chem.* **1993**, *4*, 372.
(40) Liang, J.; Edelsbrunner, H.; Woodward, C. *Protein Sci.* **1998**, *7*, 1884.
(41) Edelsbrunner, H. *Discret. Comput. Geom.* **1995**, *13*, 415.
(42) Edelsbrunner, H.; Mucke, E. P. *ACM Trans. Graph.* **1994**, *13*, 43.
(43) Mansfield, M. L.; Klushin, L. I. *Macromolecules* **1993**, *26*, 4262.
(44) Nisato, G.; Ivkov, R.; Amis, E. J. *Macromolecules* **1999**, *32*, 5895.

MA049168L